Limiting degradation mechanisms for high-temperature oxidation resistance of promising ATF cladding solutions

Martin Steinbrück, Mirco Große, Chongchong Tang, Juri Stuckert

Karlsruhe Institute of Technology (KIT), Institute for Applied Materials (IAM-AWP)
Hermann-von-Helmholtz-Platz 1, 76344 Eggenstein-Leopoldshafen, Germany
martin.steinbrueck@kit.edu
doi.org/10.13182/TopFuel22-38967

INTRODUCTION

At the latest since the accidents at Fukushima Daiichi, the need to develop new accident-tolerant materials for nuclear reactors has become apparent. One focus of international research has been on accident tolerant fuel (ATF) cladding materials because the fuel clad is a key barrier against fission product release and in contact with the cooling water and high temperature steam during accident scenarios.

The classical zirconium alloy (Zry) cladding materials, which have been developed further and further in recent decades, behave excellently under operating conditions. The fuel failure rate in currently operating water-cooled nuclear power reactors is very low and has been decreasing by tendency [1]. But during accident scenarios with temperatures beyond 1000°C, the strong reaction of Zr alloys with water steam results in the loss of barrier effect of the Zr based cladding tubes as well as significant release of hydrogen and heat, which in turn influence the progression of the accident [2] [3]. The chemical heat released by zirconium oxidation may exceed the residual nuclear decay heat after reactor shutdown, and the released hydrogen bears the risk of oxyhydrogen explosions. In this context, the focus for the development of ATF cladding materials has been on significantly improved high-temperature oxidation resistance, reducing the above-described effects and increasing the coping time for accident management measures [4] [5] [6].

Generally, the high-temperature oxidation resistance of metals, alloys, and non-oxide ceramics relies on the formation of a protective oxide scale, i.e. one of the three oxides alumina (Al_2O_3), chromia (Cr_2O_3) or silica (SiO_2) [7]. Consequently, after a decade of research, the three most promising candidates for ATF cladding are Cr-coated zirconium alloys, FeCrAl alloys and silicon carbide (SiC) based ceramic composite materials, forming chromia, alumina, and silica, respectively, at high temperature in oxidizing atmospheres.

An enormous number of papers on the development and characterization of ATF cladding materials has been published in recent years. The authors of this paper are mainly involved in the investigation of the oxidation and degradation behavior of those promising ATF cladding materials up to very high temperatures. With this experience, this paper should summarize the oxidation and degradation mechanisms of the three main ATF cladding concepts and derive the maximum "survival" temperatures under accident conditions. For each material, first, the main oxidation and degradation mechanisms are briefly discussed and then illustrative examples of results obtained at KIT are given.

CHROMIUM-COATED ZIRCONIUM ALLOYS

Cr-coated zirconium alloys are the nearest term solution for ATF cladding materials, which should be connected with only moderate changes in technology and licensing procedures. They are developed worldwide using different coating methods with typical Cr layer thicknesses of 5-30 µm. Generally, advanced Cr coatings offer very good behavior under harsh operating conditions and result in a reduction of the high-temperature oxidation kinetics by 1-2 orders of magnitude compared to Zr alloys. First lead test assemblies (LTA) are already applied in commercial reactors in the US and Europe. Recent overview papers have been published e.g. by Bischoff [8], Brachet [9] [10], Maier [11], Yeom [12] and Yang [13].

High-temperature oxidation and degradation of Cr coatings on Zr alloys

The following obvious mechanisms result in the degradation of protective effect of Cr coatings:

- The oxidation by steam resulting in a well adherent and protective Cr_2O_3 scale, but also causing consumption of the thin coating layer.
- The interaction between chromium coating and zirconium bulk results in (1) the formation of the intermetallic compound $ZrCr_2$ and (2) the diffusion of Cr into the Zr bulk, see Zr-Cr phase diagram [14] in Fig. 1. Both are leading to the consumption of the Cr coating.
- Furthermore, also according to the Zr-Cr phase diagram and (3), the eutectic interaction between Zr and Cr at 1332°C leads to the formation of melt and should characterize the ultimate upper limit for the stability of Cr coatings.
- The volatilization of the chromium oxide by the formation of gaseous species may be another consumption mechanism of the protective coating [15].

The oxidation of chromium leads to the formation of chromia, Cr_2O_3, see Eq.1.

$$2Cr + 3H_2O \rightarrow Cr_2O_3 + 3H_2 \quad (1)$$

The oxidation kinetics of chromium is mainly determined by the diffusion of metal cations through the growing oxide scale to the surface. Inward transport of oxygen ions along grain boundaries is also observed, resulting in compressive stresses by oxide formation at the metal-oxide interface or within the scale [16]. The parabolic rate constants for the oxidation of chromium in oxygen, air and steam scatter widely. This could be caused by the different contribution of inward oxygen diffusion through oxide layers with different grain sizes and textures of the investigated materials. Brachet [10] summarized literature data on the parabolic rate coefficients for the oxidation of chromium in different atmospheres and illustrated the scatter over several orders of magnitude, but also recommended a correlation for the parabolic oxidation kinetics in steam based on recent data from CEA and Framatome, see TABLE I in the discussion section.

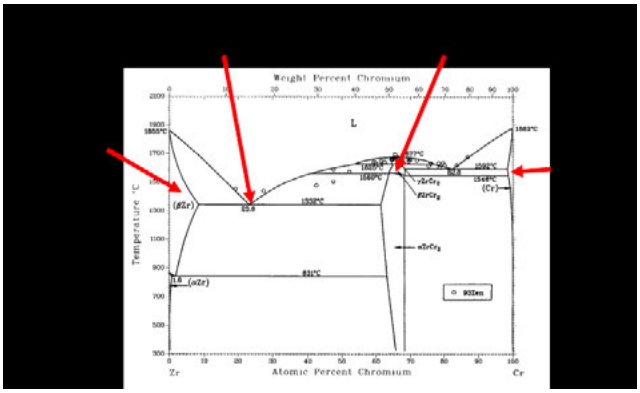

Fig. 1. Phase diagram Zr-Cr [14] and its implications on Cr coating degradation.

As already mentioned, the volatilization of the protective oxide scale may have to be taken into account at very high temperature and for longer duration, especially for chromium oxide with the highest volatilization rate among the high-temperature oxidation resistant oxides [15]. Volatilization of Cr trioxide, CrO_3, in dry oxidizing conditions and of chromium oxyhydroxides, e.g. $CrO_2(OH)_2$, in steam-rich atmospheres may cause formation of thinner oxide scales and higher metal recession than expected from the parabolic growth kinetics [17]. However, Brachet [10] investigated and discussed the volatilization of Cr_2O_3 and concluded that it can be neglected at least up to 1300°C.

Detailed investigations of the Cr coating degradation mechanisms were made by various research groups [10] [18] [19] [20]. They show, depending on temperature and Cr coating thickness/morphology, a transition from protective to non-protective behavior. In addition to the above discussed degradation effects, the main mechanism for this transition is the diffusion of zirconium along Cr grain boundaries towards the Cr/Cr_2O_3 interface and its oxidation by oxygen from the ambient and by redox reaction with the Cr oxide. Finally, a through-going network of zirconia is formed, which allows fast oxygen transport to the bulk Zr and its oxidation as illustrated in Fig. 2.

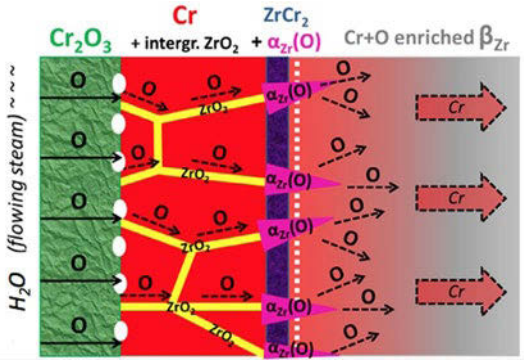

Fig. 2. Schematic view of the transition from protective to non-protective Cr coating. Taken from *[10]*.

Various authors discuss the formation of blisters/bubbles/voids during high-temperature oxidation of Cr-coatings. This could be related to the compressive stresses in the oxide because of the high Pilling-Bedworth ratio for the chromium oxidation [9]. Other mechanisms for the formation of pores of various sizes could be vacancy condensation and the reaction between Zr and Cr_2O_3 [20] or segregation of Sn and Cr in the surface region of the substrate close to the Cr coating [21].

Single rod experiments with Cr-coated fuel rod simulators

Single-rod oxidation and quench experiments were conducted in cooperation between Westinghouse, EPRI (US) and KIT (Germany) [22]. 10-cm long Optimized ZIRLO™ samples with cold-sprayed (CS) and PVD coating of different thicknesses (25 µm and 10 µm, respectively) were inductively heated in steam atmosphere and partially quenched by a rising cylinder filled with water. Fig. 3 shows for illustration such samples as coated, during testing in the QUENCH-SR facility with inductive heating, and after a transient test.

Generally, less oxidation, measured online by mass spectrometry of the hydrogen release, was observed for the coated samples compared to ZIRLO reference samples. At 1100°C, all coating remained protective for at least one hour. At 1200°C, only the thicker CS coating remained intact for one hour, whereas the thinner PVD coating started transition to non-protective behavior after approximately 20 min as can be seen in Fig. 4 (top). Towards the end of these tests, the oxidation rate of the PVD Cr-coated sample reached the same level as of the non-coated reference sample, however, the integral hydrogen release remained much lower for both coated samples.

Fig. 3. Cr-coated samples before (left), during (mid), and after transient experiment up to >1500°C.

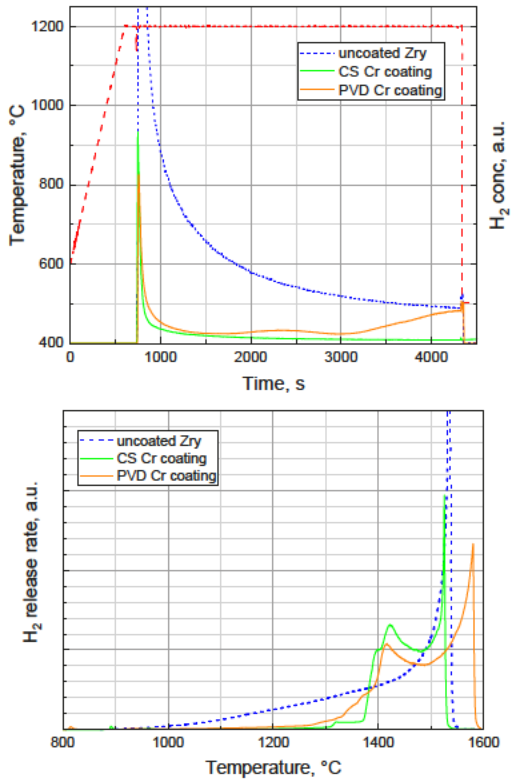

Fig. 4. Hydrogen release during isothermal tests at 1200°C (top) and transient tests up to >1500°C (bottom) with Cr-coated fuel rod simulators.

The post-test ductility was also much better for the coated sample: The uncoated sample easily broke just during handling. The Cr coating layer revealed excellent thermal shock resistance and adherence, without cracking and spallation.

In transient tests from 800°C to >1500°C, lower oxidation rates were observed, as expected, for the coated samples compared to the uncoated one up to approx. 1350°C. At higher temperature, the oxidation rate of the (formerly) coated samples became significantly higher than for the uncoated one, see Fig. 4 (bottom). This rapid increase of oxidation rate should be caused by the failure of the Cr coating after passing the eutectic temperature. The intermediate decrease of the oxidation kinetics is caused by the formation of zirconia. The second peak in oxidation kinetics at around 1500°C is due to the phase transition from tetragonal to cubic zirconia [3] [23].

Another result of this series of experiments was that pre-damage of the Cr coating by scratches caused locally increased oxidation only where the scratches passed through the Zr alloy. No delamination of the adjacent Cr scale layer was observed, and the scratches had little effect on the overall hydrogen release [22].

FECRAL ALLOYS

FeCrAl alloys are ferritic body-centred cubic (bcc) iron-based alloys with 12-24 wt.% Cr and 3-6 wt.% Al contents. Beside their potential application for ATF cladding [24] [25] [26], they are primarily used for high temperature applications such as for heating elements in industrial furnaces and for gas burners.

Oxidation of FeCrAl alloys at high temperatures

The superior oxidation resistance of FeCrAl alloys at high temperature relies on the formation of a slowly growing and highly protective α-Al_2O_3 scale. A common understanding is that α-Al_2O_3 forms on FeCrAl alloys at temperatures exceeding 900-1000°C.

Generally, all three elements of FeCrAl alloys can be oxidized by oxygen and steam resulting in the formation of the corresponding oxides; see Equ.2 for the steam oxidation.

$$2M + 3H_2O \rightarrow M_2O_3 + 3H_2 \qquad (2)$$

Al_2O_3 and Cr_2O_3 are the only stable solid oxides in the corresponding binary metal-oxygen systems. In the Fe-O system, Fe_3O_4 (magnetite) and FeO (wustite) with lower oxygen contents are known beside the sesquioxide Fe_2O_3 (hematite). All sesquioxides form solid solutions with each other with corundum or spinel-type [27]. Furthermore, ternary compounds can be formed of which the spinel-type compounds AB_2O_4 are worth to mention [28].

The thermodynamic stability of the oxides is in the order Al_2O_3>Cr_2O_3>Fe_2O_3, i.e. alumina is by far the most stable oxide forming at the lowest oxygen partial pressure, which promotes the selective oxidation of aluminum at high

temperatures. Alumina formation is also supported by Cr, as can be seen in Fig. 5 (third element effect) [29]. Several metastable aluminum oxides are known, which may also be formed during oxidation of FeCrAl alloys [30]. All forms of alumina, except α-Al_2O_3, are termed transient aluminas and are thermodynamically meta-stable, fast-growing and have fairly poor protective properties [31] [32].

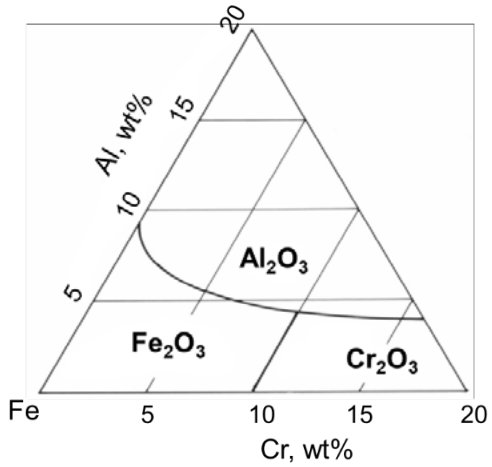

Fig. 5. Oxide map of the Al-Cr-Fe system at 1000°C, after Scheil [33].

Even if alumina formation is thermodynamically preferred, other oxides may form due to kinetic limitations during the initial transient phase and in case of too low aluminum concentration in the alloy or due to Al depletion in the bulk alloy during oxidation [34]. After the initial phase, the formation of a protective α-alumina scale is determined by the competition between the oxidation rate governed by diffusion of Al and O through the oxide scale and the diffusion of aluminum in the substrate to the interface [35]. Al is much more mobile than Fe and Cr in FeCrAl alloys at high temperatures [36], which supports the formation of protective Al_2O_3 also on alloys with relatively low Al content.

Nuclear grade iron-based FeCrAl alloys with optimized composition to perform in both normal and off-normal conditions have been mainly developed in the US [37] [38] [24] and Japan [39] [26] [40]. They usually have lower Cr contents (12-13 wt%) compared to commercial Kanthal alloys (20-22 wt%) in order to reduce neutron-irradiation induced embrittlement during operation [41]; the Al content is 5-6 wt%. In addition, FeCrAl alloys may contain minor alloying elements to improve oxidation resistance (by e.g. reactive elements), microstructure, mechanical properties, and processability as well as ODS (oxide dispersed strengthened) particles [26] [42] [43].

Recent results on oxidation mechanisms and kinetics of FeCrAl alloys show only a moderate dependence of the parabolic rate constants on the alloy composition as long as a protective alumina scale is formed in the temperature range of approximately 1000-1400°C [25] [44] [45]. A recommended correlation based on data of Pint [4] is given in TABLE I. At lower temperatures, the oxidation kinetics is determined by the formation of Al-rich transient oxides, and it is therefore 2-3 orders of magnitude higher than the extrapolated correlation for α-alumina, see Fig. 6. However, this has only a limited effect on accident scenarios because of the generally low level of oxidation rates between 600°C and 900°C. Of higher importance in this context is the tendency of nuclear grade FeCrAl alloys to undergo transition to catastrophic oxidation already from 1300-1400°C, i.e. at lower temperatures compared to the commercial Kanthal alloys APM and APMT. As shown in Fig. 6, the by five orders of magnitude higher oxidation rates at these conditions correlate with the kinetics of iron oxide formation [45], and it results usually in fast and complete oxidation of FeCrAl samples. The onset of catastrophic oxidation is dependent on alloy composition and heating rate with earlier transition for high heating rates [44].

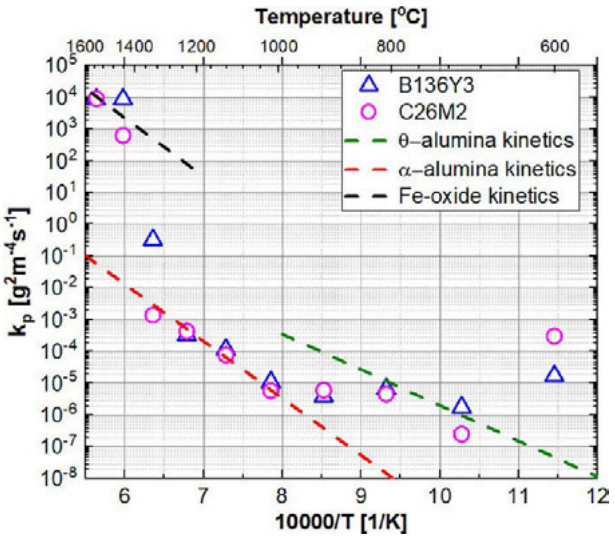

Fig. 6. Parabolic rate constants of nuclear grade alloys B136Y3 and C26M2 as a function of temperature with the parabolic correlations of Fe-oxide, α-alumina and θ-alumina. Taken from [45].

The volatilization of aluminum oxide in steam is very low and it should not play a significant role as long as the oxidation is determined by a protective α-alumina scale [15].

Main results of the bundle experiment QUENCH-19

The first large-scale bundle test with ATF cladding material, namely with the FeCrAl alloy B136Y3 (Century Tubes Inc. /ORNL), was conducted in the QUENCH facility at KIT in cooperation with ORNL, USA, in 2018 [46]. This facility is a large-scale bundle facility with 24 electrically heated, >2 m long fuel rod simulators [2], see Fig. 7 (left). It is extensively instrumented with high-temperature thermocouples, pressure gauges, level meters, etc., and coupled with a mass spectrometer for analysis of hydrogen

and other gases. Usually, experiments are completed by reflooding (which gave the facility the name). The QUENCH-19 experiment with FeCrAl cladding was run with a very similar scenario as test QUENCH-15 with uncoated ZIRLO cladding with respect to bundle geometry and power input. The FeCrAl experiment was run 2000 s longer at the highest power input, until first local melting of the FeCrAl cladding was expected. Hence, the FeCrAl bundle was quenched 2000 s later than the ZIRLO bundle.

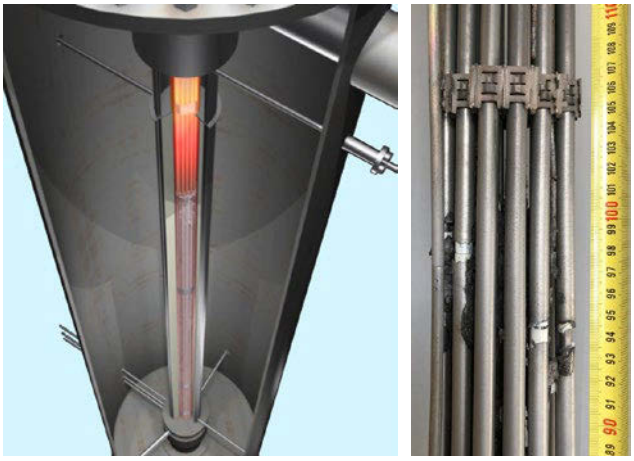

Fig. 7. Schematic of the QUENCH facility during reflood phase (left) and post-test view of the FrCrAl bundle after experiment QUENCH-19.

As expected, the hydrogen release was much less in the FeCrAl experiment: Until the time when the QUENCH-15 test was terminated by reflood, 100x less hydrogen was produced in the QUENCH-19 experiments (0.4 g and 40 g, respectively), see Fig. 8. Even at the end of the QUENCH-19 test after 2000 s longer heating time at the highest power level, only 9 g hydrogen were measured compared to 47 g in the shorter test with ZIRLO.

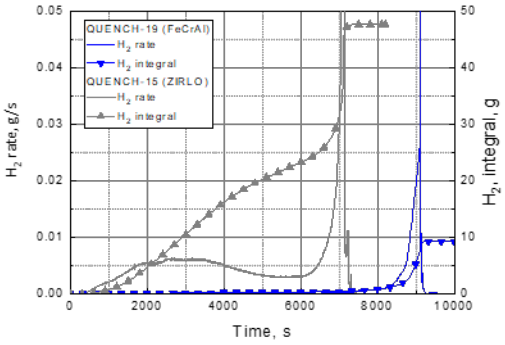

Fig. 8. Hydrogen release during experiment QUENCH-19 (FeCrAl) and reference test QUENCH-15 (ZIRLO).

Some melt formation was seen in the bundle after the test, which also came from stainless steel (SS 304) thermocouple sheaths. Rupture of some cladding tubes was observed most probably caused by strong shrinking during the quench phase due to the two times higher thermal expansion coefficient of FeCrAl compared to Zr alloys, Fig. 7. Only low oxidation of the FeCrAl surfaces unaffected by melt attack was seen along the whole bundle.

Post-test calculations in the framework of the IAEA project ACTOF resulted in much too low values of the hydrogen release during the test [47]. One important reason for this is that the codes used only one correlation for the oxidation of FeCrAl alloy resulting in an underestimation of the hydrogen release below and above the validity temperature region for α-alumina formation.

SILICON CARBIDE COMPOSITES

Silicon carbide ceramics are intensively studied for application as heating elements and high-temperature structural materials e.g. gas turbines, space travel and in nuclear industry. They offer excellent high-temperature mechanical properties, low density as well as high oxidation and irradiation resistance. Silicon carbide composites are considered a promising long-term candidate for ATF cladding tubes in LWRs [48] [49] [50].

High temperatures oxidation and degradation of SiC

The oxidation of SiC is more complex compared e.g. to the oxidation of zirconium alloys. Generally, its high-temperature oxidation resistance relies on the formation of a protective SiO_2 scale [50]. Many different phases of SiC as well as of SiO_2 exist, which is not further discussed here.

In dry atmospheres, like oxygen or air, passive oxidation with the formation of a protective silica scale (see Equ.3) or active oxidation with the formation of gaseous silicon monoxide (Equ.4)) may take place, depending on temperature and oxygen partial pressure. The rate controlling process for passive oxidation is the diffusion of oxygen through the growing oxide scale [51]. It is observed at high oxygen partial pressure and lower temperature [52] [53]. Active oxidation may be an issue for instance for high-temperature application of SiC components in technical helium cooling gas with oxidizing impurities [54].

$$SiC + 2O_2 \rightarrow SiO_2 + CO_2 \quad (3)$$
$$SiC + O_2 \rightarrow SiO(g) + CO \quad (4)$$

A protective silica scale is also produced during oxidation of silicon carbide in steam-containing atmosphere, see Equ.5 and TABLE I. Hydrogen is released in addition to carbon-containing gases. At very high temperatures, the formation of volatile hydroxides or oxyhydroxides may become significant, e.g. according to Equ.6 and Equ.7. Formation and volatilization of a silica scale at the same time finally lead to paralinear oxidation kinetics as illustrated in Fig. 9.

$$SiC + 3H_2O \rightarrow SiO_2 + CO + 3H_2 \quad (5)$$

$$SiO_2 + 2H_2O \rightarrow Si(OH)_4 \quad (6)$$
$$SiO_2 + H_2O \rightarrow SiO(OH)_2 \quad (7)$$

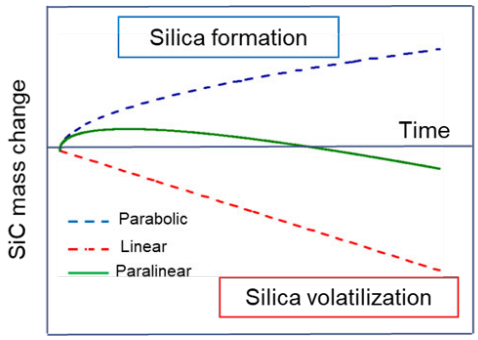

Fig. 9. Paralinear mass change during HT oxidation in steam of SiC due to formation and volatilization of a superficial SiO_2 scale.

Many authors observed formation of bubbles in the silica scale especially during high-temperature oxidation in steam containing atmospheres [55] [56] [57] [58] [59]. Pressure can build up by the formation of CO and H_2 if the permeability of inward diffusing oxidizing species is higher than of the outward moving gaseous reaction products. The tendency for bubble formation increases with temperature and increasing steam partial pressure. However, the effect of bubble formation on the overall oxidation kinetics does not seem to be too important.

Impurities in the furnace, the sample, or the oxidizing atmosphere might strongly affect oxidation kinetics [60]. This is one of the reasons why published data on high-temperature oxidation of silicon carbide are so scattered. The oxidation process is accelerated by the presence of impurities and residual sintering additives, which affect the microstructure of the protective SiO_2 scale.

SiC ceramic matrix composites (CMC) itself, consisting of SiC fibers typically coated with pyrolytic carbon (PyC) in a SiC matrix have only a limited high-temperature oxidation resistance [61] [62] [57]. The carbon layer is easily oxidized and the CMC provides a large surface for oxidation. Therefore, all SiC CMC based cladding tube designs contain a superficial monolithic SiC environmental barrier coating (EBC) or seal-coat [57] [63] [49].

An upper temperature limit for a reasonable oxidation resistance should be given by the melting temperature of the formed silica scale at around 1725°C, but for a short period, also higher temperatures have been reported without severe degradation of SiC-based cladding tube segments [58].

Single rod experiments with SiC CMC cladding segments

Isothermal oxidation tests and one transient experiment in steam until failure were conducted with SiC CMC cladding tube segments produced by CEA (France) in the QUENCH-SR facility at KIT [64] [65]. The samples were filled with graphite rods acting as susceptor for inductive heating, see Fig. 10.

The isothermal tests ran at 1700 °C for one and three hours, respectively, and were mostly terminated by quenching with water. Even though formation of bubbles was observed during the experiments, all samples survived the harsh test conditions with only slight modification of the surface, Fig. 10. The surface was covered by 1-3 µm thick silica scales. Mechanical properties were only slightly degraded.

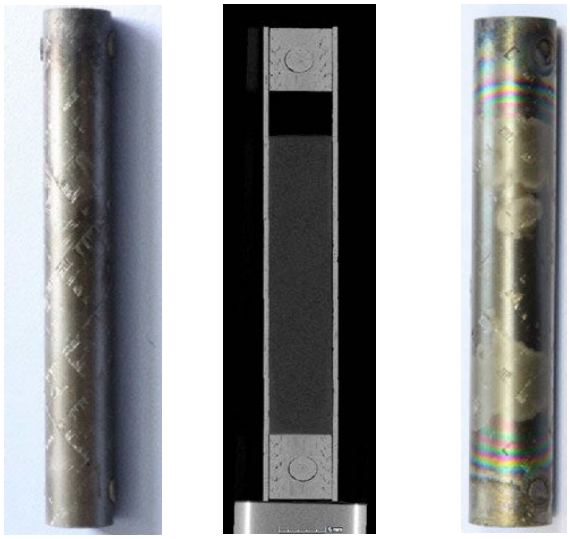

Fig. 10. SiC CMC samples as received (left), X-ray tomography showing end plugs and graphite core (mid), and after 1 hour steam oxidation at 1700°C (right).

The release of gaseous reaction products, mainly H_2, CO_2 and CO was measured in-situ by mass spectrometry. Rather constant low release of all these gases established soon (1-3 min) after initiating the steam injection. This indicated a quick establishment of an equilibrium of silica formation (parabolic kinetics) and volatilization (linear kinetics) at these conditions. Based on the hydrogen release data, the SiC recession rate was estimated to be 15-25 µm/h under the conditions of these experiments (T = 1700°C, P = 1 bar, P_{H2O} = 0.65 bar, and F_{gas} = 5 cm/s).

A transient test with 10 K/min heating rate in steam was conducted from 1400°C until failure of the sample, defined by strongly increasing gas release rates and formation of white smoke. As shown in Fig. 11, the gas release rates (i.e. oxidation rate) increased up to approximately 1500°C and then remained nearly constant up to 1700°C, before increasing dramatically by a factor of 20 at about 1820°C. This transition was most probably caused by the (local) failure of the protective SiC seal-coat and the steam attack of the fiber-matrix composite, as can be seen in Fig. 12.

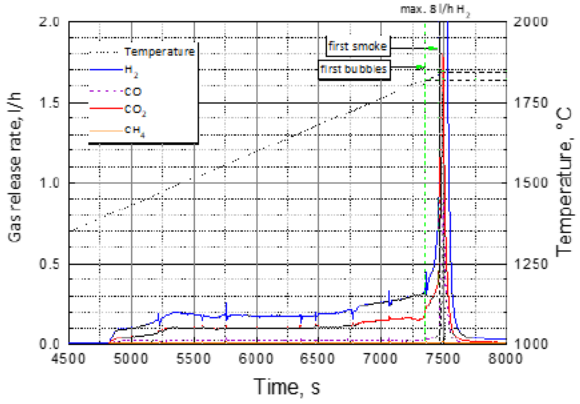

Fig. 11. Temperature and gas release during transient test.

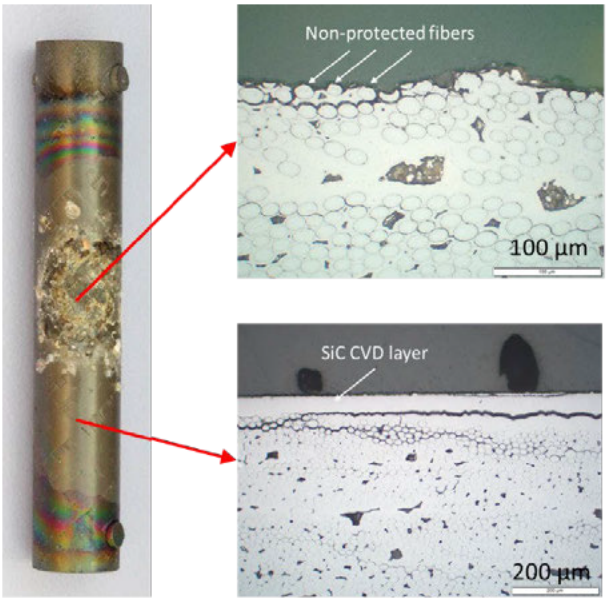

Fig. 12. Post-test appearance of the SiC-CMC sample after the transient test up to >1800°C.

DISCUSSION

The high-temperature oxidation resistance of the three most promising ATF cladding concepts relies on the formation of one of the protective oxides alumina, chromia and silica. This agrees to the generally accepted knowledge of high-temperature oxidation behavior of materials. The growth kinetics of these oxides can be described by parabolic correlations e.g. according to Equ.8+9, with d_{ox} oxide thickness, t time, K_0 pre-exponential constant, E_A activation energy, gas constant R=8.314 J/Kmol, and T temperature.

$$d_{ox} = K_p \cdot \sqrt{t} \qquad (8)$$

$$K_p = K_0 \cdot exp\left(-\frac{E_A}{RT}\right) \qquad (9)$$

TABLE I and Fig. 13 provide data for the parabolic rate constants selected from literature for comparison. These correlations are not universally valid, because they cover only a certain temperature range or a special material, but they illustrate the improved oxidation kinetics of the ATF cladding materials compared to Zry and can be used for first estimation of expected oxide thickness at given temperature and time. Furthermore, these correlations do not take into account the volatilization of oxides, especially of silica [66] and possibly of chromia for temperatures higher than the protective behavior of Cr coatings [67]. The volatilization kinetics of oxides is strongly dependent on thermal-hydraulic boundary conditions, and its detailed discussion is beyond the scope of this paper. Typical oxide thicknesses on Zr alloys at severe accident conditions are >100 µm, about 10 µm chromia and around 1 µm alumina or silica are observed in high-temperature tests of ATF cladding materials.

TABLE I. Parabolic rate constants for the oxidation of ATF cladding materials (oxide scale thickness)

Material	K_0 $m/s^{0.5}$	E_A J/molK	Remark	Ref.
Zry-4	1.50 E-3	75100	tetragonal ZrO_2	[68]
Cr	2.69 E-3	120000		[10]
FeCrAl	1.50 E-2	172000	α-Al_2O_3 on APMT	[4]
SiC	4.95 E-5	119000		[57]

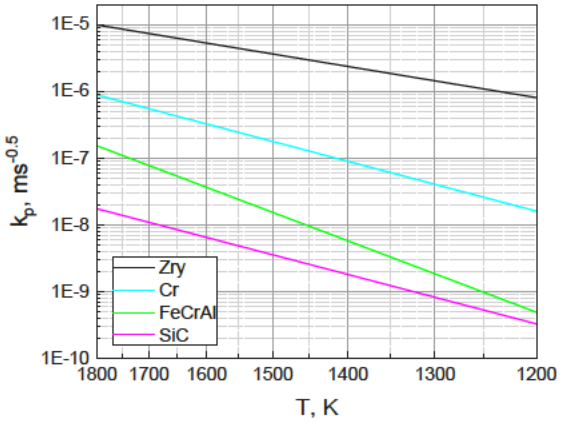

Fig. 13. Arrhenius plot of the parabolic rate constants for the oxidation of ATF cladding materials. Correlations taken from TABLE 1.

The degradation mechanisms, and with it the maximum application/survival temperatures significantly differ between the three ATF cladding concepts.

The protective effect of the Cr-coated zirconium alloys is not only affected by the oxidation of the chromium but also by interactions between Cr coating and Zry bulk as discussed above. The ultimately limiting mechanism is the eutectic melt formation in the system Cr-Zr at 1332°C. At lower temperature, the thickness of the Cr coating plays an important role; thicker Cr layers provide a higher chromium

reservoir and usually longer withstand high-temperature conditions without losing their protective effect [69]. A recent study [70] showed the preservation of the protective effect of a 90 µm Cr coating at 1300°C for one hour, while thinner and for ATF cladding application more prototypic coatings showed a transition to non-protective behavior at 1200°C already after about 30 min [20] [22]. Beside the thickness of the Cr coating, its quality and morphology does also affect the protectiveness of the coating [9] [69] [71]. Chromia volatility seems not play a role for the degradation of the coating for the temperature range discussed here and the relatively short durations of hours considered for nuclear accident scenarios. A serious problem for any type of coating on Zr alloys can be a possible temperature runaway after loss of protective effect of the coating and the consequent intense Zr-steam reaction. The investigation of this effect will be one of the objectives of the OECD-NEA Joint Undertaking QUENCH-ATF [72].

Nuclear grade FeCrAl alloys should have low Cr and Al contents for optimized radiation resistance. Low Cr and Al contents can impair the HT oxidation resistance; therefore, a compromise must eventually be found. Nuclear grade FeCrAl alloys generally show a better high-temperature oxidation resistance in steam than commercial Kanthal alloys at intermediate temperatures of 1000-1300°C, but tend to suffer catastrophic oxidation at higher temperatures of around 1400°C [38] [45]. The transition temperature to catastrophic oxidation is quite stochastic even under very similar conditions and needs further investigation. It seems to be dependent on composition, morphology, and surface finish of the cladding as well as of the heating rate and other boundary conditions.

The high-temperature oxidation resistance of SiC based composites for nuclear cladding relies on the formation of a protective silica scale on the monolithic external SiC layer. The fiber matrix composite itself has low resistance to oxidation mainly due to the interphase between fiber and matrix that is usually made of carbon. The limited number of publications on the oxidation behavior of SiC-based cladding at very high temperatures seems to confirm high oxidation resistance up to at least 1700°C lasting for several hours. At that high temperature, volatilization of the formed silica scale as well as bubble formation must be taken into account as degradation mechanisms. Generally, the oxidation of SiC materials is strongly dependent on impurities (in material and atmosphere) as well as on experimental conditions (pressure, gas flow rates, gas composition). This complicates the comparison of data obtained in different labs and explains the wide scatter of published data.

CONCLUSION

This paper summarized oxidation and degradation of the three most promising ATF cladding concepts, discussed the limiting mechanisms for protection at very high temperatures, and provided an illustrative example of each from experimental work at KIT.

All ATF claddings discussed in this paper provide strongly improved high-temperature oxidation resistance compared to classical zirconium alloys. They could contribute to decrease the risk of temperature escalation and hydrogen detonation during severe accidents as well as significantly increase the coping time for accident management measures. The maximum survival temperatures for the ATF cladding materials are:

- 1200-1300°C for Cr-coated Zry
- around 1400°C for nuclear grade FeCrAl alloys
- >1700°C for SiC_f-SiC composites with monolithic external SiC layer

However, various issues with all of these materials must be solved for successful introduction in NPP fuel elements.

REFERENCES

[1] V. Inozemtsev and V. Onufriev, "Results of the IAEA study of fuel failures in water cooled reactors in 2006-2010," in *LWR Fuel Performance Meeting, Top Fuel 2013*, 2013.

[2] M. Steinbrück, M. Große, L. Sepold and J. Stuckert, "Synopsis and outcome of the QUENCH experimental program," *Nuclear Engineering and Design,* vol. 240, pp. 1714-1727, 2010.

[3] M. Steinbrück, "High-Temperature Oxidation of Zirconium Alloys in Various Atmospheres," in *Encyclopedia of Materials: Metals and Alloys*, vol. 1, F. G. Caballero, Ed., Oxford, Elsevier, 2022, p. 454–463.

[4] B. Pint, K. Terrani, Yamamoto, Y. and L. Snead, "Material Selection for Accident Tolerant Fuel Cladding," *Metallurgical and Materials Transactions E,* vol. 2, pp. 190-196, 2015.

[5] K. Terrani, "Accident tolerant fuel cladding development: Promise, status, and challenges," *Journal of Nuclear Materials,* vol. 501, pp. 13-30, 2018.

[6] C. Tang, M. Stueber, H. Seifert and M. Steinbrueck, "Protective coatings on zirconium-based alloys as accident-Tolerant fuel (ATF) claddings," *Corrosion Reviews,* vol. 35, pp. 141-165, 2017.

[7] D. J. Young, High Temperature Oxidation and Corrosion of Metals, Elsevier Ltd., 2016.

[8] J. Bischoff, C. Delafoy, C. Vauglin, P. Barberis, C. Roubeyrie, D. Perche, D. Duthoo, F. Schuster, J.-C. Brachet, E. Schweitzer and K. Nimishakavi, "AREVA NP's enhanced accident-tolerant fuel developments: Focus on Cr-coated M5 cladding," *Nuclear Engineering and Technology,* vol. 50, pp. 223-228, 2018.

[9] J.-C. Brachet, I. Idarraga-Trujillo, M. Flem, M. Saux, V. Vandenberghe, S. Urvoy, E. Rouesne, T. Guilbert, C. Toffolon-Masclet, M. Tupin, C. Phalippou, F. Lomello, F. Schuster, A. Billard, G. Velisa, C. Ducros and F. Sanchette, "Early studies on Cr-Coated Zircaloy-4 as enhanced accident tolerant nuclear fuel claddings for light water reactors," *Journal of Nuclear Materials,* vol. 517, pp. 268-285, 2019.

[10] J.-C. Brachet, E. Rouesne, J. Ribis, T. Guilbert, S. Urvoy, G. Nony, C. Toffolon-Masclet, M. Le Saux, N. Chaabane, H. Palancher, A. David, J. Bischoff, J. Augereau and E. Pouillier, "High temperature steam oxidation of chromium-coated

zirconium-based alloys: Kinetics and process," *Corrosion Science,* vol. 167, art. no. 108537, 2020.

[11] B. Maier, H. J. Yeom, G., T. Dabney, J. Walters, J. Romero, H. Shah, P. Xu and K. Sridharan, "Development of Cold Spray Coatings for Accident-Tolerant Fuel Cladding in Light Water Reactors," *JOM,* vol. 70, pp. 198-202, 2018.

[12] H. Yeom, B. Maier, G. Johnson, T. Dabney, M. Lenling and K. Sridharan, "High temperature oxidation and microstructural evolution of cold spray chromium coatings on Zircaloy-4 in steam environments," *Journal of Nuclear Materials,* vol. 526, art. no. 151737, 2019.

[13] J. Yang, M. Steinbrück, C. Tang, M. Große, J. Liu, J. Zhang, D. Yun and S. Wang, "Review on chromium coated zirconium alloy accident tolerant fuel cladding," *Journal of Alloys and Compounds,* vol. 895, art. no. 162450, 2022.

[14] D. Arias and J. Abriata, "The Cr-Zr (Chromium-Zirconium) system," *Bulletin of Alloy Phase Diagrams,* vol. 7, pp. 237-244, 1986.

[15] P. Meschter, E. Opila and N. Jacobson, "Water Vapor-Mediated Volatilization of High-Temperature Materials," *Annual Review of Materials Research,* vol. 43, pp. 559-588, 2013.

[16] N. Birks, G. Meier and F. Pettit, Introduction to the High Temperature Oxidation of Metals, 2nd ed., Cambridge University Press, 2006.

[17] M. Stanislowski, E. Wessel, K. Hilpert, T. Markus and L. Singheiser, "Chromium vaporization from high-temperature alloys," *Journal of the Electrochemical Society,* vol. 154, pp. A295-A306, 2007.

[18] X. Han, C. Chen, Y. Tan, W. Feng, S. Peng and H. Zhang, "A systematic study of the oxidation behavior of Cr coatings on Zry4 substrates in high temperature steam environment," *Corrosion Science,* vol. 174, art. no. 108826, 2020.

[19] J. Liu, C. Tang, M. Steinbrück, J. Yang, U. Stegmaier, M. Große, D. Yun and H. Seifert, "Transient experiments on oxidation and degradation of Cr-coated Zircaloy in steam up to 1600°C," *Corrosion Science,* vol. 192, art. no. 109805, 2021.

[20] J. Liu, M. Steinbrück, M. Große, U. Stegmaier, C. Tang, D. Yun, J. Yang, Y. Cui and H. Seifert, "Systematic investigations on the coating degradation mechanism during the steam oxidation of Cr-coated Zry-4 at 1200 °C," *Corrosion Science,* vol. 202, art. no. 110310, 2022.

[21] X. Hu, C. Dong, Q. Wang, B. Chen, Yang, W. T. H., R. Zhang, W. Gu and D. Chen, "High-temperature oxidation of thick Cr coating prepared by arc deposition for accident tolerant fuel claddings," *Journal of Nuclear Materials,* vol. 519, pp. 145-156, 2019.

[22] M. Steinbrück, U. Stegmaier, M. Große, L. Czerniak, E. Lahoda, R. Daum and K. Yueh, "High-temperature oxidation and quenching of chromium-coated zirconium alloy ATF cladding tubes with and w/o pre-damage," *Journal of Nuclear Materials,* art. no. 153470, 2022.

[23] M. Steinbrück, "Oxidation of zirconium alloys in oxygen at high temperatures up to 1600 °C," *Oxidation of Metals,* vol. 70, pp. 317-329, 2008.

[24] S. Dryepondt, K. Unocic, D. Hoelzer, C. Massey and B. Pint, "Development of low-Cr ODS FeCrAl alloys for accident-tolerant fuel cladding," *Journal of Nuclear Materials,* vol. 501, pp. 59-71, 2018.

[25] K. Field, M. Snead, Y. Yamamoto and K. Terrani, "Handbook on the Materials Properties of FeCrAl Alloys for Nuclear Power Production Applications," ORNL/SPR-2018/905, 2018.

[26] K. Sakamoto and Y. Miura, "Progress on Japanese Development of Accident Tolerant FeCrAl-ODS Fuel Claddings for BWRs," in *Proceedings of the TOPFUEL 2018 Conference*, 2018.

[27] J. Gallardo Amores, V. Sanchez Escribano and G. Busca, "Characterization of Fe-Cr-Al mixed oxides," *Materials Chemistry and Physics,* vol. 60, 1999.

[28] K. Lipkina, D. Hallatt, E. Geiger, B. Fitzpatrick, K. Sakamoto, H. Shibata and M. Piro, "A study of the oxidation behaviour of FeCrAl-ODS in air and steam environments up to 1400 °C," *Journal of Nuclear Materials,* vol. 541, art. no. 152305, 2020.

[29] E. N. E. Airiskallio, M. Heinonen, I. Väyrynen, K. Kokko, M. Ropo, M. Punkkinen, H. Pitkänen, M. Alatalo, J. Kollár, B. Johansson and L. Vitos, "Third element effect in the surface zone of Fe-Cr-Al alloys," *Physical Review B - Condensed Matter and Materials Physics,* vol. 81, art. no. 033105, 2010.

[30] K. Prasanna, A. Khanna, R. Chandra and W. Quaakkers, "Effect of θ-alumina formation on the growth kinetics of alumina-forming superalloys," *Oxidation of Metals,* vol. 46, pp. 465-480, 1996.

[31] G. Rybicki and J. Smialek, "Effect of the θ-α-Al2O3 transformation on the oxidation behavior of β-NiAl + Zr," *Oxidation of Metals,* vol. 31, pp. 275-304, 1989.

[32] H. El Kadiri, R. Molins, Y. Bienvenu and M. Horstemeyer, "Abnormal high growth rates of metastable aluminas on FeCrAl alloys," *Oxidation of Metals,* vol. 64, pp. 63-97, 2005.

[33] E. Scheil and E. Schulz, "Hitzebeständige Chrom-Aluminium Stähle," *Archiv für das Eisenhüttenwesen,* vol. 6, pp. 155-160, 1932.

[34] N. Israelsson, "High Temperature Oxidation and Chlorination of FeCrAl alloys," Chalmers university of Technology, Göteborg, Sweden, 2014.

[35] B. Lesage, L. Maréchal, Huntz, A.-M. and R. Molins, "Aluminium depletion in FeCrAl alloys during oxidation," *Defect and Diffusion Forum,* Vols. 194-199, pp. 1707-1712, 2001.

[36] D. Rohrberg, K.-H. Spitzer, L. Dörrer, P. Tankeu, M. Podsiadlo, G. Borchardt, T. Markus and R. Schmid-Fetzer, "Interdiffusion in ternary Fe-Cr-Al alloys with variable molar volume," *Materials at High Temperatures,* vol. 25, pp. 247-255, 2008.

[37] Y. Yamamoto, B. Pint, K. Terrani, K. Field, Y. Yang and L. Snead, "Development and property evaluation of nuclear grade wrought FeCrAl fuel cladding for light water reactors," *Journal of Nuclear Materials,* vol. 467, pp. 703-716, 2015.

[38] B. Pint, "Performance of FeCrAl for accident-tolerant fuel cladding in high-temperature steam," *Corrosion Reviews,* vol. 35, pp. 167-175, 2017.

[39] F. Nagase, K. Sakamoto and S. Yamashita, "Performance degradation of candidate accident-Tolerant cladding under corrosive environment," *Corrosion Reviews,* vol. 35, pp. 129-140, 2017.

[40] K. Sakamoto, Y. Miura, S. Ukai, A. Kimura, A. Yamaji, K. Kusagaya and S. Yamashita, "Recent progress in development of accident tolerant fecral-Ods fuel claddings for BWRs in Japan," in *GLOBAL 2019 - International Nuclear Fuel Cycle Conference and TOP FUEL 2019 - Light Water Reactor Fuel Performance Conference*, 2020.

[41] K. Field, X. Hu, K. Littrell, Y. Yamamoto and L. Snead, "Radiation tolerance of neutron-irradiated model Fe–Cr–Al alloys," *Journal of Nuclear Materials,* vol. 465, pp. 746-755, 2015.

[42] B. A. Pint, A. J. Garratt-Reed and L. W. Hobbs, "The reactive element effect in commercial ODS FeCrAI alloys," *Materials at High Temperatures,* vol. 13, pp. 3-16, 1995.

[43] D. Naumenko, B. Pint and W. Quadakkers, "Current Thoughts on Reactive Element Effects in Alumina-Forming Systems," *Oxidation of Metals,* vol. 86, pp. 1-43, 2016.

[44] C. Tang, A. Jianu, M. Steinbrueck, M. Grosse, A. Weisenburger and H. Seifert, "Influence of composition and heating schedules on compatibility of FeCrAl alloys with high-temperature steam," *Journal of Nuclear Materials,* vol. 511, pp. 496-507, 2018.

[45] C. Kim, C. Tang, M. Grosse, Y. Maeng, C. Jang and M. Steinbrueck, "Oxidation mechanism and kinetics of nuclear-grade FeCrAl alloys in the temperature range of 500–1500 °C in steam," *Journal of Nuclear Materials,* art. no. 153696, 2022.

[46] J. Stuckert, M. Grosse, M. Steinbrueck and K. Terrani, "Results of the bundle test QUENCH-19 with FeCrAl claddings," in *GLOBAL 2019 - International Nuclear Fuel Cycle Conference and TOP FUEL 2019 - Light Water Reactor Fuel Performance Conference*, 2020.

[47] IAEA, "Final Report: Analysis of Options and Experimental Examination of Fuels for Water Cooled Reactors with Increased Accident Tolerance (ACTOF)," IAEA-TECDOC-1921, 2020.

[48] L. Snead, T. Nozawa, Y. Katoh, T.-S. Byun, S. Kondo and D. Petti, "Handbook of SiC properties for fuel performance modeling," *Journal of Nuclear Materials,* vol. 371, pp. 329-377, 2007.

[49] J. Braun, C. Sauder, J. Lamon and F. Balbaud-Célérier, "Influence of an original manufacturing process on the properties and microstructure of SiC/SiC tubular composites," *Composites Part A: Applied Science and Manufacturing,* vol. 123, pp. 170-179, 2019.

[50] H. Pham, M. Kurata and M. Steinbrueck, "Steam Oxidation of Silicon Carbide at High Temperatures for the Application as Accident Tolerant Fuel Cladding, an Overview," *Thermo,* vol. 1, pp. 151-167, 2021.

[51] B. Deal and A. Grove, "General relationship for the thermal oxidation of silicon," *Journal of Applied Physics,* vol. 36, pp. 3770-3778, 1965.

[52] N. Jacobson, B. Harder and D. Myers, "Oxidation transitions for SiC part I. Active-to-passive transitions," *Journal of the American Ceramic Society,* vol. 96, pp. 838-844, 2013.

[53] B. Harder, N. Jacobson and D. Myers, "Oxidation transitions for sic part II. Passive-to-active transitions," *Journal of the American Ceramic Society,* vol. 96, pp. 606-612, 2013.

[54] M. Steinbrueck, V. Angelici Avincola, I. Markel, U. Stegmaier, Gerhards and S. H. U., "Oxidation of SiC f -SiC CMC cladding tubes for GFR application in impure helium atmosphere and materials interactions with tantalum liner at high temperatures up to 1600°C," *Journal of Nuclear Materials,* vol. 517, pp. 337-348, 2019.

[55] B. Schneider, A. Guette, R. Naslain, M. Cataldi and A. Costecalde, "A theoretical and experimental approach to the active-to-passive transition in the oxidation of silicon carbide: Experiments at high temperatures and low total pressures," *Journal of Materials Science,* vol. 33, pp. 535-547, 1998.

[56] E. Opila, "Variation of the Oxidation Rate of Silicon Carbide with Water-Vapor Pressure," *Journal of the American Ceramic Society,* vol. 82, pp. 625-636, 1999.

[57] K. Terrani, B. Pint, C. Parish, C. Silva, L. Snead and Y. Katoh, "Silicon carbide oxidation in steam up to 2 MPa," *Journal of the American Ceramic Society,* vol. 97, pp. 2331-2352, 2014.

[58] V. Angelici Avincola, M. Grosse, U. Stegmaier, M. Steinbrueck and H. Seifert, "Oxidation at high temperatures in steam atmosphere and quench of silicon carbide composites for nuclear application," *Nuclear Engineering and Design,* vol. 295, p. 468–478, 2015.

[59] H. Pham, Y. Nagae, M. Kurata, D. Bottomley and K. Furumoto, "Oxidation kinetics of silicon carbide in steam at temperature range of 1400 to 1800 °C studied by laser heating," *Journal of Nuclear Materials,* vol. 529, art. no. 151939, 2020.

[60] E. Opila and N. Jacobson, "Oxidation and Corrosion of Ceramics," in *Ceramics Science and Technology*, Wiley, 2013.

[61] H. Kleykamp, V. Schauer and A. Skokan, "Oxidation behaviour of SiC fibre reinforced SiC," *Journal of Nuclear Materials,* vol. 227, pp. 130-137, 1995.

[62] C. Cabet, "Review: Oxidation of SiC/SiC composites in low oxidising and high temperature environment," *NATO Science for Peace and Security Series B: Physics and Biophysics,* pp. 351-366, 2008.

[63] L. Chaffron, C. Sauder, C. Lorrette, L. Briottet, A. Michaux, L. Gélébart, A. Coupé, M. Zabiego, M. Le Flem and J.-L. Séran, "Innovative SiC/SiC composite for nuclear applications," in *EPJ Web of Conferences 51, Art. No. 01003*, 2013.

[64] M. Steinbrück, M. Große, U. Stegmaier, J. Braun and C. Lorrette, "High-temperature oxidation of silicon carbide composites for nuclear applications," in *Proceedings of the TOPFUEL 2021 Conference*, Santander, Spain, 2021.

[65] M. Steinbrück, M. Große, U. Stegmaier, J. Braun and C. Lorrette, "Oxidation of silicon carbide composites for nuclear applications at very high temperatures in steam," *Coatings,* vol. submitted, 2022.

[66] V. Angelici Avincola, D. Cupid and H. Seifert, "Thermodynamic modeling of the silica volatilization in steam related to silicon carbide oxidation," *Journal of the European Ceramic Society,* vol. 35, pp. 3809-3818, 2015.

[67] D. Young and B. Pint, "Chromium volatilization rates from Cr2O3 scales into flowing gases containing water vapor," *Oxidation of Metals,* vol. 66, pp. 137-153, 2006.

[68] J. Cathcart, R. Pawel, R. McKee, R. Druschel, G. Yurek, J. Campbell and S. Jury, "Zirconium metal-water oxidation kinetics IV. Reaction rate studies," ORNL/NUREG-17, ORNL, USA, 1977.

[69] E. Kashkarov, D. Sidelev, M. Syrtanov, C. Tang and M. Steinbrück, "Oxidation kinetics of Cr-coated zirconium alloy: Effect of coating thickness and microstructure," *Corrosion Science,* vol. 175, art. no. 108883, 2020.

[70] Q. Li, P. Song, R. Zhang, Z. Li, Y. Wang, P. Du and J. Lu, "Oxidation behavior and Cr-Zr diffusion of Cr coatings prepared by atmospheric plasma spraying on zircaloy-4 cladding in steam at 1300 °C," *Corrosion Science,* vol. 203, art. no. 110378, 2022.

[71] W. Wang, G. Zhang, C. Wang, T. Wang and T. Li, "Construction of chromium coatings with (200) preferred orientation and exploration the high-temperature steam oxidation properties," *Journal of Nuclear Materials,* vol. 563, art. no. 153660.

[72] OECD-NEA, "QUENCH-ATF project," 2020. [Online]. Available: https://www.oecd-nea.org/jcms/pl_36597/quench-atf-project.